**Pharmaceutical Sciences and Drug Design**
**ISSN: 3062-4428**
2021, Volume 1, Page No: 146-163

Available online at: www.galaxypub.co/page/journals

**Galaxy Publication**

# Novel 1,2,3-Triazole-Urea Conjugates as Potent and Liver-Selective Antiproliferative Agents: Synthesis, Biological Evaluation, and Mechanistic Insights

**Samuel Mensah[1]*, Kojo Asare[1]**

[1]Department of Biotechnology, Faculty of Science, University of Ghana, Accra, Ghana.

***E-mail** ✉ samuel.mensah.gh@gmail.com

**Received:** 14 September 2021; **Revised:** 27 November 2021; **Accepted:** 03 December 2021

## ABSTRACT

The need for effective targeted agents against hepatocellular carcinoma remains pressing. This investigation focused on designing and examining a new panel of triazole–urea hybrid molecules for potential anticancer activity. A collection of urea derivatives containing terminal alkynes was generated using a combined assembly and modification route. These intermediates were subsequently transformed through Click chemistry to afford novel triazole–urea hybrids (3a–3e, 5a–5e, 7a–7e). Their growth-inhibitory effects were evaluated via the CCK-8 assay against several human tumor cell lines (lung: H460, H1299, A549, PC-9; liver: Huh-7; breast: MCF-7) and normal hepatocytes (L02). Mechanistic analyses included apoptosis induction, autophagy markers, and DNA damage responses. An acute toxicity assessment was carried out in female KM mice at an oral dose of 500 mg/kg, with continuous monitoring of body mass, organ indices, and histological changes in primary organs. Most synthesized molecules showed marked, dose- and time-dependent suppression of Huh-7 cell proliferation, while only minor activity was detected in other malignant lines. Importantly, none displayed toxicity toward L02 normal liver cells. Mechanistic assays confirmed that the lead candidate triggered apoptotic processes, autophagic responses, and DNA damage in Huh-7 cells. In vivo, no treatment-related deaths or notable alterations in weight, organ coefficients, or tissue histology were observed during the 14-day evaluation at 500 mg/kg, indicating a high tolerated dose and favorable initial safety characteristics. These outcomes highlight the selective anti-hepatoma activity and promising safety of the triazole–urea scaffold, especially compound 3c, supporting its potential for further development against hepatocellular carcinoma.

**Keywords:** 1,2,3-triazoles, Urea derivatives, Liver cancer, Anticancer properties

**How to Cite This Article:** Mensah S, Asare K. Novel 1,2,3-Triazole-Urea Conjugates as Potent and Liver-Selective Antiproliferative Agents: Synthesis, Biological Evaluation, and Mechanistic Insights. Pharm Sci Drug Des. 2021;1:146-63. https://doi.org/10.51847/JRuyOmqpSg

## Introduction

Cancer continues to be a major global health challenge, with therapeutic resistance severely diminishing treatment success [1, 2]. China bears a substantial cancer burden and records the world's highest cancer-related mortality. In 2020, cancers accounted for roughly 9.96 million deaths globally, with 30% originating from China, emphasizing the demand for new therapeutic strategies [3]. Although many factors contribute to treatment failure, classical chemotherapy is particularly hindered by resistance mechanisms [4, 5]. Hence, it is crucial to explore new compounds with alternative modes of action to overcome these barriers [6].

For decades, 1,2,3-triazoles have attracted medicinal chemists due to their ease of preparation via click chemistry and their diverse pharmacological functions [7]. This heterocyclic fragment is found in numerous bioactive agents, including antimicrobials, antiviral agents, antiallergy medications, anti-tuberculosis compounds, and various anti-inflammatory drugs [7]. Recently, interest in exploiting 1,2,3-triazoles within oncology has grown rapidly, as their incorporation into hybrid structures is expected to yield valuable anticancer leads [8, 9].

The triazole ring is a five-membered aromatic heterocycle exhibiting low basicity, occurring as 1,2,3-triazole or 1,2,4-triazole isomers. Nitrogen atoms within the structure can serve as hydrogen-bond acceptors, and the NH moiety can act as a donor, enabling interaction with biological macromolecules. Polarity resulting from carbon–

nitrogen electronegativity differences generally decreases logP values, frequently improving aqueous solubility. Triazoles also show favorable metabolic robustness [10].

Urea functional groups are widely utilized in drug design for improving interactions with targets and fine-tuning physicochemical properties [11]. Molecules containing urea often exhibit superior selectivity and enhanced metabolic stability, making them suitable frameworks to counteract therapeutic resistance [12]. Molecular hybridization—covalently merging two or more bioactive components into a single scaffold—offers an efficient strategy to generate highly potent molecules [13, 14]. Such hybrids can modulate multiple signaling routes, providing a path to bypass resistance pathways [15]. This approach may achieve synergistic action while minimizing off-target toxicity, a principle validated by recent advancements in anticancer agents [16].

Considerable recent progress illustrates the promise of hybridization. Haval and colleagues synthesized quinoline–1,2,3-triazole constructs via CuAAC reactions [17, 18]. Several displayed pronounced cytotoxicity toward MCF-7 cells, with IC50 values reaching 0.39 μg/mL—superior to doxorubicin—and exhibited favorable drug-likeness, ADMET behavior, and strong CDK2 binding supported by DFT and docking analyses. Liu *et al*. later developed 1,2,3-triazole–pyrimidine–urea hybrids **(Figure 1a)**, active against MGC-803, EC-109, MCF-7, and B16-F10 lines; notably, one compound suppressed B16-F10 with an IC50 of 32 nM and induced dose-dependent apoptosis [19]. A Sanofi derivative **(Figure 1b)** emerged as a potent and selective MET receptor tyrosine kinase inhibitor, demonstrating nanomolar activity (IC50 = 4.2 nM) and selective growth inhibition in MET-amplified tumors [20]. Cravatt's group introduced a piperidinyl 1,2,3-triazourea ABHD6 inhibitor **(Figure 1c)**, achieving nanomolar-level cellular degradation with KT185 showing exceptional in vivo selectivity [21]. Further contributions include Liu's 1,2,3-triazole–dithiocarbamate–urea analogues **(Figures 1d and 1e)**, which exhibited broad-spectrum potency (IC50 for IVa: 1.62–20.84 μM; IVb: 0.76–13.55 μM) [22]. Mao's IDO1 inhibitor **(Figure 1f)**, integrating a urea group with a 1,2,3-triazole core, produced strong enzymatic inhibition (IC50 = 0.75 μM) through enhanced target binding [23].

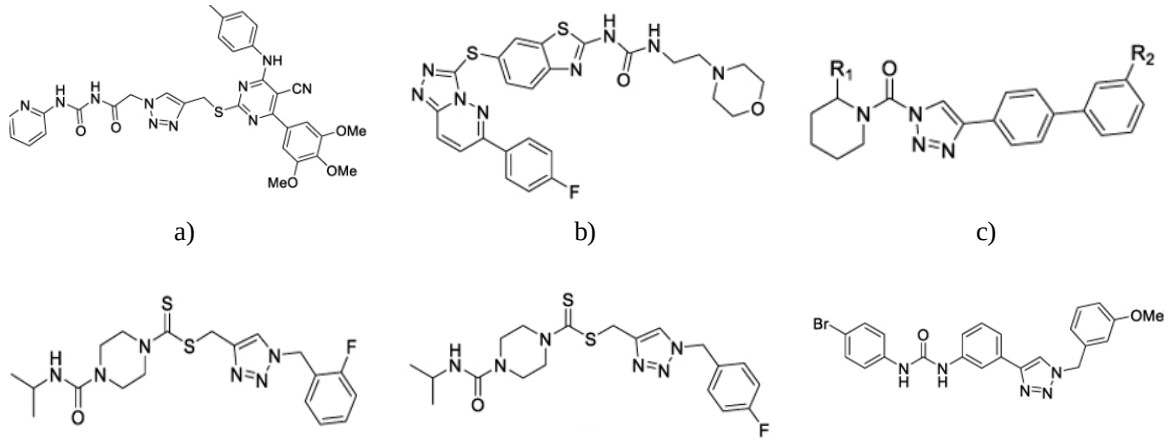


**Figure 1.** The chemical structures of the 1,2,3-triazole–urea hybrid molecules.

Although the 1,2,3-triazole–based frameworks discussed above exhibit strong potential in precision cancer therapy, most efforts have centered on refining selectivity toward a single therapeutic target. To more effectively counter the multifaceted nature of tumor drug resistance, our goal was to generate new hybrid molecules capable of engaging multiple pathways. In this work, we introduce a previously unreported molecular entity that strategically integrates a 1,2,3-triazole ring with a urea fragment. The urea unit was selected due to its prevalence in numerous biologically active structures and its strong hydrogen-bonding capacity with protein targets. We anticipated that this hybrid design would produce complementary effects, potentially bypassing resistance mechanisms associated with pure triazole inhibitors while enhancing antitumor potency through different target interactions.

Building on earlier findings where gefitinib-based 1,2,3-triazole derivatives exhibited broad anticancer responses [24, 25], we proposed that merging the triazole scaffold with a urea motif could deliver cooperative antitumor activity in drug-resistant cancers. Here, we present the design, synthesis, and biological evaluation of new

triazole–urea conjugates aimed at resistant tumor types. Our systematic study highlights selective inhibitory activity toward hepatocellular carcinoma, mediated through multimodal mechanisms, reinforced by favorable in vivo safety outcomes.

*Chemistry*

Following our previous research,23,24 we prepared a group of new molecules combining a 1,2,3-triazole core with a urea segment. Three categories of linkers—m-phenyl, p-phenyl, and methyl groups—were chosen to bridge the urea region with the triazole scaffold. Synthetic routes for the three compound sets (3a–3e, 5a–5e, 7a–7e) are presented in **Figure 2 and Table 1**. Variable substituents (R1, R2, R3, R4, R5) were introduced onto the benzene ring of phenyl isocyanates and onto benzyl fragments. Comparative analyses were carried out to evaluate how the linker substituents R1–R5 affected activity in selected human cancer cell lines.

**Table 1.** R-group variations for compounds 3a–3e, 5a–5e, and 7a–7e.

| Compound | $R^1$ | $R^2$ | $R^3$ | $R^4$ | $R^5$ |
|---|---|---|---|---|---|
| 3a | Cl | H | H | H | Cl |
| 3b | Cl | H | H | Cl | H |
| 3c | Cl | H | H | H | Br |
| 3d | H | Br | H | H | Cl |
| 3e | H | Br | H | H | Br |
| 5a | Cl | H | H | H | Cl |
| 5b | Cl | H | H | Cl | H |
| 5c | Cl | H | H | H | Br |
| 5d | H | Br | H | H | Cl |
| 5e | H | Br | H | H | Br |
| 7a | Cl | H | H | H | Cl |
| 7b | Cl | H | H | Cl | H |
| 7c | Cl | H | H | H | Br |
| 7d | H | Br | H | H | Cl |
| 7e | H | Br | H | H | Br |

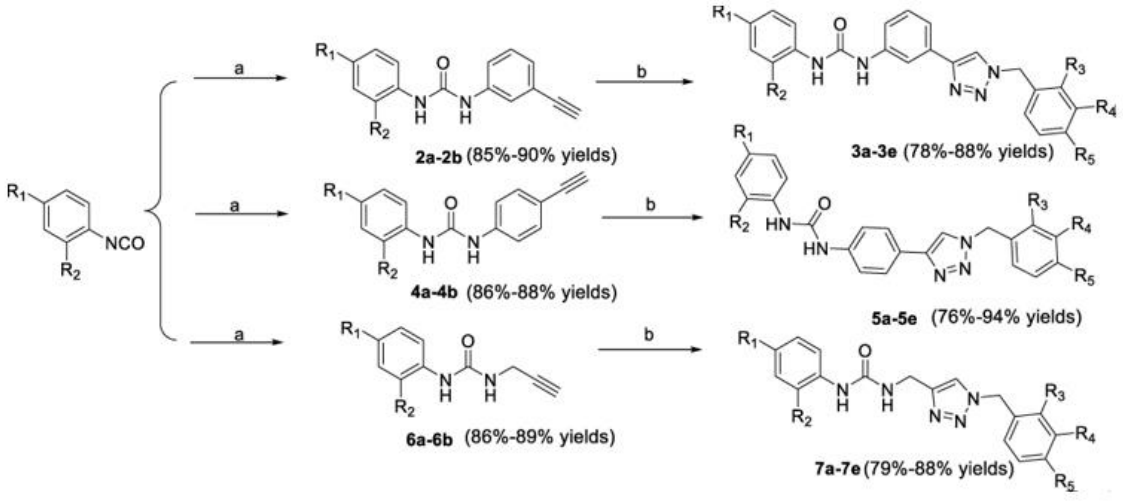


**Figure 2.** Synthetic pathways to compounds 3a–3e, 5a–5e, and 7a–7e.

*Effects of compounds 3a–3e, 5a–5e, and 7a–7e on tumor cell viability and cytotoxicity*

To assess antitumor activity, each compound was tested against various human cancer cell lines—lung (H460, H1299, A549, PC-9), liver (Huh-7), and breast (MCF-7)—at 20 μM and 50 μM, with L02 normal hepatocytes used as a control. The CCK-8 assay was performed after 48 h or 72 h, as shown in **Table 2**.

**Table 2.** Cell viability and cytotoxicity of compounds 3a–3e, 5a–5e, and 7a–7e on human lung cancer cell lines.

| Compound | H460 | H1299 | A549 | A549 | PC-9 | PC-9 |
|---|---|---|---|---|---|---|
| | 50 μM, 72 h | 50 μM, 72 h | 50 μM, 72 h | 20 μM, 72 h | 50 μM, 72 h | 20 μM, 72 h |
| 3a | 72.03 ± 1.93 | 76.26 ± 14.26 | 101.44 ± 1.93 | 121.39 ± 6.44 | 110 ± 6.52 | 95.40 ± 1.83 |
| 3b | 88.71 ± 1.56 | 103.60 ± 10.83 | 166.34 ± 4.24 | 114.55 ± 8.33 | 117.63 ± 3.89 | 102.16 ± 7.50 |
| 3c | 61.39 ± 0.78 | 76.66 ± 8.20 | 122.92 ± 7.18 | 108.07 ± 9.57 | 127.63 ± 5.02 | 85.97 ± 4.11 |
| 3d | 65.29 ± 5.19 | 130.33 ± 1.08 | 148.92 ± 25.57 | 158.77 ± 16.71 | 107.37 ± 6.27 | 130.28 ± 4.98 |
| 3e | 46.74 ± 4.50 | 108.25 ± 3.15 | 70.94 ± 5.81 | 130.05 ± 3.43 | 92.63 ± 1.47 | 127.79 ± 2.24 |
| 5a | 86.32 ± 5.28 | 88.13 ± 2.37 | 79.61 ± 3.83 | 73.16 ± 3.26 | 81.30 ± 2.01 | 85.98 ± 5.69 |
| 5b | 69.30 ± 1.45 | 82.80 ± 0.23 | 73.15 ± 1.94 | 64.62 ± 1.69 | 76.41 ± 1.82 | 72.06 ± 1.23 |
| 5c | 82.21 ± 0.89 | 89.87 ± 3.30 | 78.81 ± 1.42 | 69.12 ± 0.72 | 80.44 ± 2.54 | 71.50 ± 1.22 |
| 5d | 74.93 ± 4.42 | 109.33 ± 2.15 | 106.75 ± 1.22 | 102.47 ± 1.57 | 102.88 ± 2.78 | 98.31 ± 5.01 |
| 5e | 81.40 ± 4.92 | 115.33 ± 2.93 | 88.98 ± 3.16 | 77.29 ± 3.08 | 105.94 ± 9.45 | 85.04 ± 3.34 |
| 7a | 73.19 ± 0.35 | 82.27 ± 4.39 | 67.63 ± 2.98 | 61.69 ± 2.21 | 81.69 ± 3.31 | 83.16 ± 0.73 |
| 7b | 88.46 ± 2.41 | 91.60 ± 1.62 | 79.54 ± 5.81 | 76.69 ± 6.46 | 90.03 ± 4.17 | 90.87 ± 3.42 |
| 7c | 87.65 ± 1.38 | 91.47 ± 0.67 | 96.99 ± 4.42 | 102.40 ± 4.84 | 178.62 ± 5.90 | 111.19 ± 3.96 |
| 7d | 61.61 ± 5.53 | 90.67 ± 1.50 | 86.07 ± 2.46 | 86.36 ± 1.03 | 126.75 ± 10.69 | 94.54 ± 0.43 |
| 7e | 63.39 ± 2.15 | 89.20 ± 0.83 | 91.51 ± 1.83 | 88.83 ± 1.55 | 162.70 ± 5.67 | 99.25 ± 0.66 |
| 5-FU | 35.30 ± 1.58 | 32.54 ± 0.87 | 28.12 ± 0.73 | 35.36 ± 1.63 | 32.07 ± 1.37 | 48.49 ± 0.19 |

Compounds in the 3a–3e series produced strong growth-inhibitory activity in Huh-7 hepatocellular carcinoma cells at 50 μM following 72 h of exposure. These molecules produced notably higher inhibition percentages relative to the control group, demonstrating considerable antiproliferative capacity. By contrast, their effects on MCF-7 and L02 cells under identical conditions were minimal, indicating selective action toward Huh-7 cells.

When directly compared with the reference drug 5-FU under matching conditions (50 μM, 72 h), 5-FU displayed substantially weaker inhibition of Huh-7 cells. Quantitative evaluation from **Table 3** confirms that the newly synthesized derivatives produced significantly greater growth suppression than 5-FU across several cancer models, with Huh-7 cells showing the most prominent difference. These observations collectively support the compounds' heightened selectivity and potency against hepatic cancer cells.

**Table 3.** Viability and cytotoxicity of compounds 3a–3e, 5a–5e, and 7a–7e in Huh-7, MCF-7, and L02 cells.

| Compound | Huh-7 | Huh-7 | MCF-7 | L02 | L02 |
|---|---|---|---|---|---|
| | 50 μM, 48 h | 50 μM, 72 h | 50 μM, 72 h | 50 μM, 48 h | 50 μM, 72 h |
| 3a | 84.05 ± 6.96 | 15.60 ± 4.19 | 103.82 ± 0.52 | 98.15 ± 0.33 | 101.53 ± 3.20 |
| 3b | 73.71 ± 2.02 | 14.99 ± 1.74 | 92.31 ± 3.39 | 70.47 ± 2.18 | 71.79 ± 2.49 |
| 3c | 60.53 ± 1.40 | 13.09 ± 2.47 | 96.54 ± 1.02 | 86.79 ± 3.30 | 97.38 ± 3.01 |
| 3d | 53.11 ± 0.76 | 11.16 ± 0.22 | 89.47 ± 2.26 | 69.62 ± 0.48 | 62.19 ± 5.21 |
| 3e | 61.25 ± 2.65 | 10.79 ± 0.38 | 89.74 ± 0.40 | 76.79 ± 0.96 | 45.21 ± 3.98 |
| 5a | 83.63 ± 5.51 | 72.81 ± 6.41 | 94.60 ± 0.95 | 97.98 ± 0.53 | 109.78 ± 3.32 |
| 5b | 86.69 ± 3.72 | 70.37 ± 1.73 | 91.80 ± 0.13 | 98.20 ± 3.54 | 92.59 ± 0.66 |

| | | | | | |
|---|---|---|---|---|---|
| 5c | 98.39 ± 2.16 | 64.97 ± 1.20 | 93.68 ± 1.32 | 97.83 ± 1.52 | 107.35 ± 1.40 |
| 5d | 80.25 ± 6.13 | 87.22 ± 4.09 | 99.33 ± 2.76 | 104.30 ± 0.28 | 112.55 ± 11.33 |
| 5e | 70.79 ± 4.40 | 72.81 ± 2.87 | 92.90 ± 0.55 | 103.16 ± 2.23 | 103.80 ± 0.11 |
| 7a | 65.70 ± 0.65 | 60.49 ± 2.19 | 80.75 ± 2.83 | 83.30 ± 1.25 | 126.60 ± 11.54 |
| 7b | 86.07 ± 6.06 | 82.18 ± 7.45 | 82.00 ± 2.22 | 87.20 ± 2.91 | 99.97 ± 2.81 |
| 7c | 88.20 ± 4.82 | 87.88 ± 1.35 | 89.80 ± 2.64 | 91.17 ± 1.78 | 140.67 ± 2.81 |
| 7d | 66.27 ± 1.56 | 65.58 ± 0.22 | 84.41 ± 1.62 | 88.63 ± 0.38 | 117.25 ± 0.76 |
| 7e | 61.23 ± 3.60 | 72.91 ± 1.03 | 84.69 ± 0.91 | 80.24 ± 1.24 | 106.98 ± 0.44 |
| 5-FU | 50.52 ± 2.38 | 44.39 ± 1.48 | 96.45 ± 1.20 | 88.13 ± 0.71 | 98.98 ± 2.09 |

Next, IC50 values for each compound in Huh-7 cells were measured following 72 h incubation. Cell viability was determined by CCK-8 analysis after treatment with graded dose ranges. Inhibition percentages were generated from viability data, and IC50 values were calculated via nonlinear regression of the dose–response curves. These findings, along with statistical metrics, are detailed in **Table 4**.

**Table 4.** IC50 values of the designed derivatives against Huh-7 cells.

| **Compound** | **$IC_{50}$ (μM)** | **Compound** | **$IC_{50}$ (μM)** | **Compound** | **$IC_{50}$ (μM)** |
|---|---|---|---|---|---|
| | Huh-7 | | Huh-7 | | Huh-7 |
| 3a | 13.04 ± 0.10 | 5a | >50 | 7a | >50 |
| 3b | 15.13 ± 0.09 | 5b | >50 | 7b | >50 |
| 3c | 10.23 ± 1.32 | 5c | >50 | 7c | >50 |
| 3d | 13.50 ± 0.59 | 5d | >50 | 7d | >50 |
| 3e | 12.25 ± 1.31 | 5e | >50 | 7e | >50 |
| 5-FU | 38.98 ± 0.56 | | | | |

The IC50 determinations revealed that all members of the 3a–3e group displayed inhibitory concentrations below 15 μM in Huh-7 cultures. Among them, 3c showed the strongest suppression (IC50 = 10.23 ± 1.32 μM), followed by 3e, which also demonstrated notable potency (IC50 = 12.25 ± 1.31 μM). In contrast, compounds belonging to series 5a–5e and 7a–7e consistently exhibited IC50 values exceeding 50 μM. These findings illustrate that introducing an m-phenyl spacer between the urea segment and the triazole moiety substantially enhances the biological effect compared with the p-phenyl and methyl linkers.

To pinpoint how this structural feature influences performance, analogues with identical substituent patterns were evaluated in direct comparison sets: (3a, 5a, 7a), (3b, 5b, 7b), (3c, 5c, 7c), (3d, 5d, 7d), and (3e, 5e, 7e). Examining these matched groups consistently reinforced the conclusion that the m-phenyl connection provides the most pronounced functional advantage.

The reference compound 5-FU served as the positive control and produced an IC50 of 38.98 ± 0.56 μM, highlighting that the 3-series derivatives surpass this benchmark and further validating the beneficial influence of the m-phenyl bridge. Overall, these outcomes offer direction for optimizing linker design in subsequent iterations of structural refinement.

*Antiproliferative effects of compounds 3c and 3e (Live/dead staining)*

Cell viability was visualized using a Calcein-AM/Propidium Iodide assay. Huh-7 cells were exposed to 5, 10, and 20 μM concentrations of compounds 3c or 3e and incubated for 24 h in 96-well plates. Afterward, Calcein-AM and PI were added, allowed to react for 1 hour in the dark, and imaging was performed using confocal fluorescence microscopy. As shown in **Figure 3**, higher concentrations led to a progressive increase in PI-positive (nonviable) cells and a decline in Calcein-AM fluorescence, demonstrating dose-dependent growth inhibition.

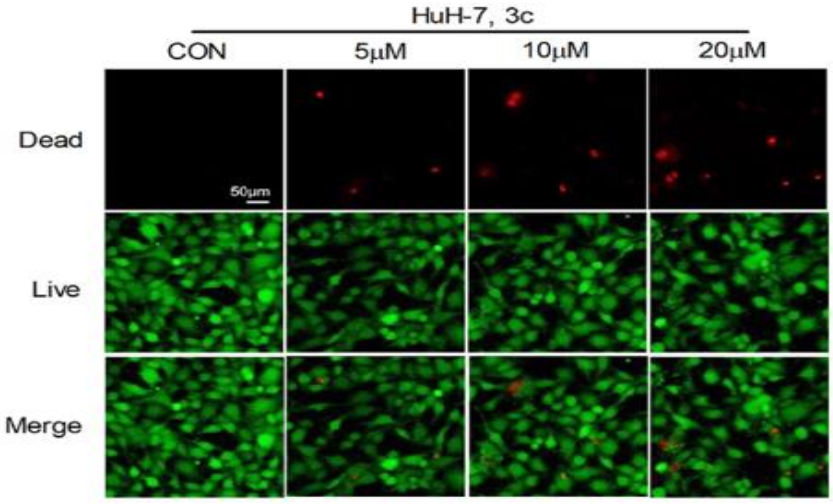


a)

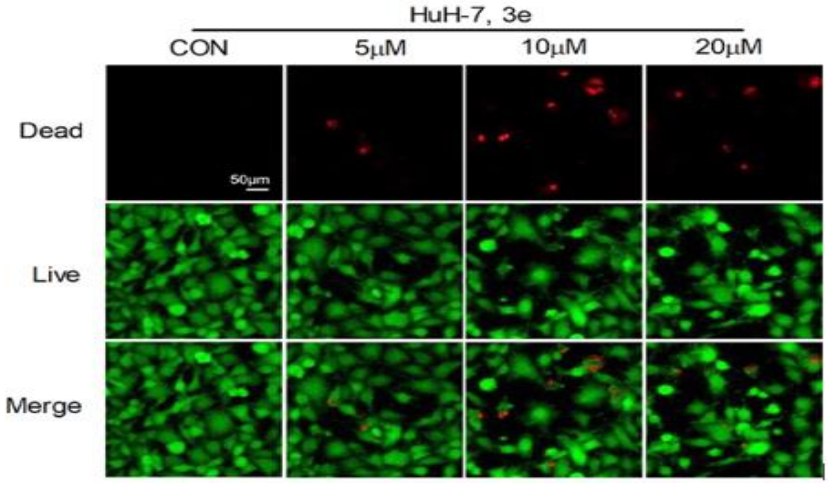


b)

**Figure 3.** Live/dead imaging following 24 h treatment.
(a) Huh-7 cells treated with 3c.
(b) Huh-7 cells treated with 3e.
n = 5–6.

*Apoptotic response induced by compounds 3c and 3e*

Programmed cell death was quantified using flow cytometry after exposing Huh-7 cells to 5, 10, and 20 μM of either compound 3c or 3e for 72 h. Harvested cells were stained with Annexin V-FITC and PI, allowing discrimination of necrotic (Q1), late apoptotic (Q2), early apoptotic (Q3), and viable (Q4) compartments. As illustrated in **Figures 4a and 4b**, apoptosis increased substantially in a concentration-dependent fashion for both compounds.

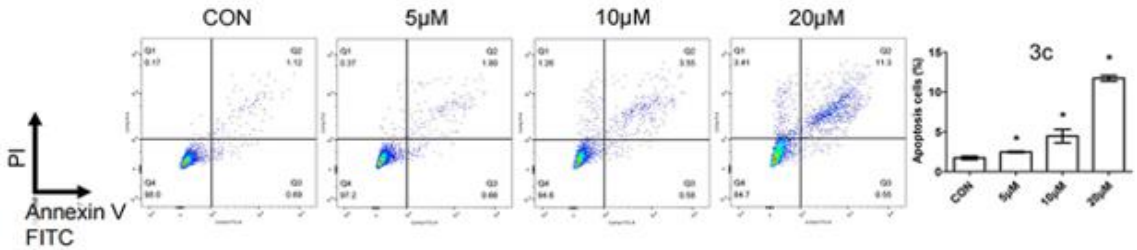


a)

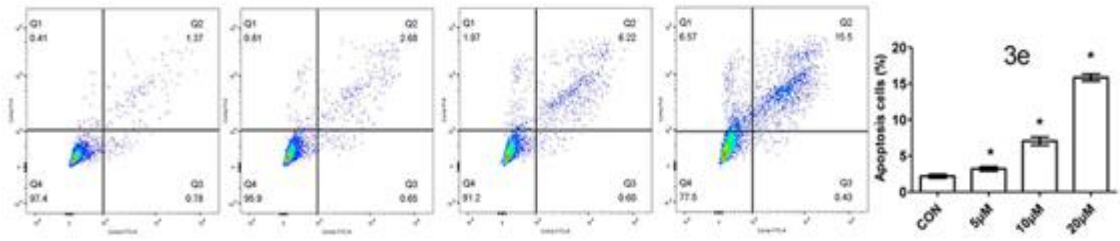


b)

**Figure 4.** Flow cytometric analysis after 72 h exposure.
(a) Apoptosis profile for 3c (5, 10, 20 μM).
(b) Apoptosis profile for 3e (5, 10, 20 μM).
Values reported as Mean ± SE.
Statistics: one-way ANOVA with Dunnett's correction.
*P < 0.05.
n = 5.

*Modulation of cell-death-related gene transcripts by 3c and 3e*

To explore molecular pathways affected by these compounds, Huh-7 cells were treated with 10 μM of either 3c or 3e. After 72 h, total RNA was isolated and quantitative RT-PCR was performed to examine transcripts associated with oxidative stress, apoptosis, DNA damage, and autophagy.

For 3c, a distinct rise in Keap1 transcript abundance was detected. However, genes tied to oxidative balance (Nrf2, Gpx4, TNFa), damage response (p53, p21, H2AX), programmed cell death (Bcl2, caspase6, caspase7), and autophagic processes (ATG5, ATG7) remained essentially unchanged **(Figure 5a)**.

For 3e, a notable elevation of Bcl2 was observed along with increases in Gpx4 and TNFa, implicating oxidative and survival-related pathways. Markers associated with DNA injury and autophagy remained unaltered **(Figure 5b)**.

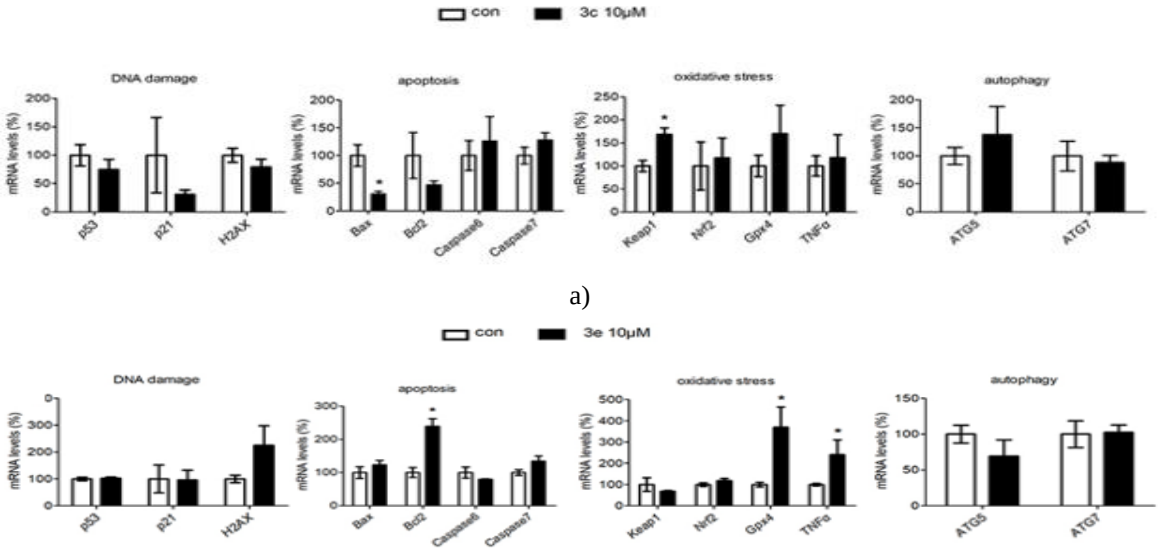


a)




b)

**Figure 5.** Gene-expression changes after 72 h exposure.
(a) Relative mRNA levels for P53, P21, H2AX, Bax, Bcl2, caspase6, caspase7, Keap1, Nrf2, Gpx4, TNFa, ATG5, ATG7 in cells treated with 3c.
(b) Same gene panel following 3e treatment.
Data shown as Mean ± SEM.
Statistics: two-tailed Student's t-test.
*P < 0.05.
n = 6.

*Effects of compounds 3c and 3e on protein expression*

To clarify how the two derivatives influence proteins associated with different cell-death pathways, Huh-7 cultures were exposed to 10 μM of either 3c or 3e for 72 h. Total protein extracts were then prepared for analysis. After treatment with 3c, a noticeable rise in LC3—a central indicator of autophagosome formation—was observed under both evaluated conditions **(Figures 6a and 6b)**. In contrast, exposure to 3e led to a pronounced elevation of H2AX, a DNA-damage-responsive marker, while most other protein targets displayed little to no change or were reduced **(Figure 6b)**.

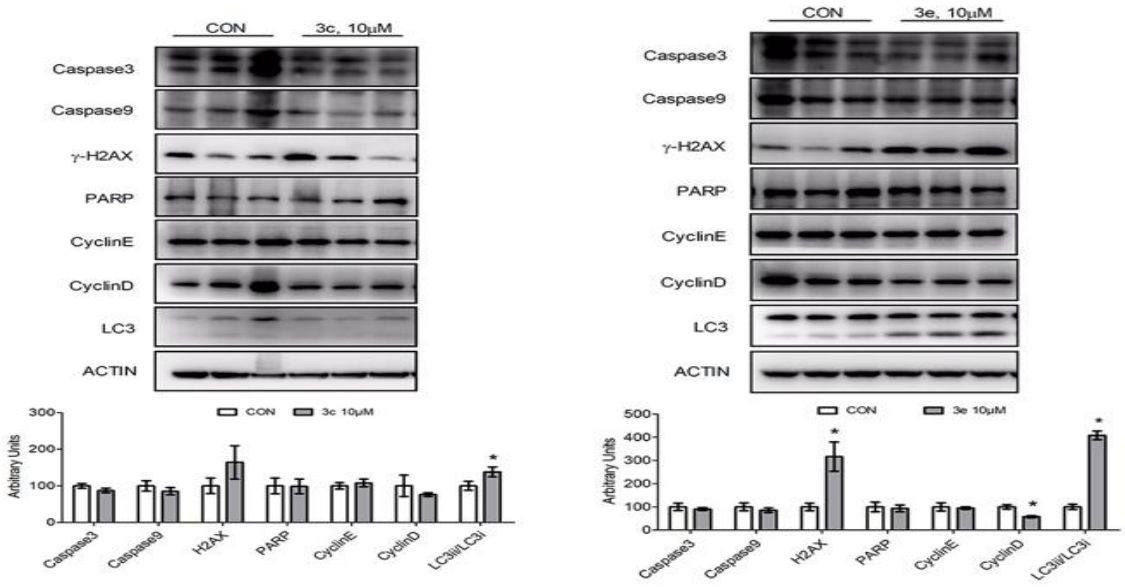


a) b)

**Figure 6.** (a) Western blot profiles of caspase 3, caspase 9, γ-H2AX, PARP, Cyclin D, Cyclin E, and LC3 in Huh-7 cells treated with compound 3c for 72 h.

(b) Same protein panel assessed in cells treated with compound 3e for 72 h.

All quantitative data shown as Mean ± SEM, tested using a two-tailed Student's t-test, $P < 0.05$, $n = 6$.

*Compounds 3c and 3e induce DNA damage in tumor cells*

To determine whether these molecules compromise genomic integrity, Huh-7 cells were incubated with 5, 10, or 20 μM of each compound for 24 h and later processed with a DNA-damage detection kit. The trends matched the protein results: both 3c and 3e triggered incremental, concentration-dependent increases in DNA injury **(Figure 7)**. These outcomes are consistent with the idea that the rigid, planar 1,2,3-triazole–urea framework may insert between DNA bases, thereby provoking structural disruption and subsequently promoting cell death. The strong response seen in Huh-7 cells may relate to this line's atypical DNA-repair characteristics.

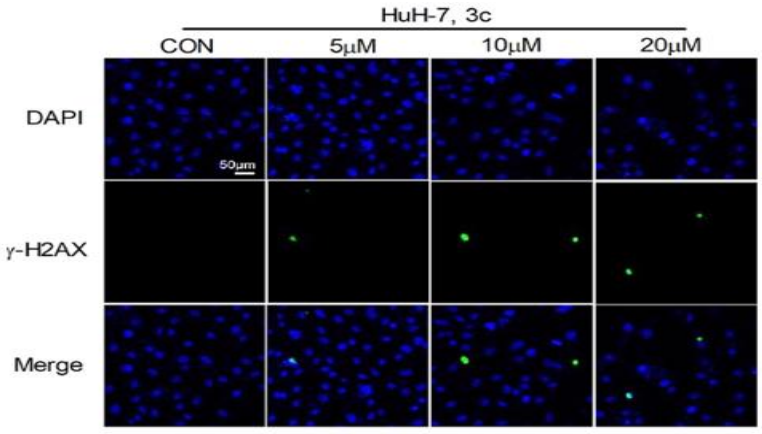


a)

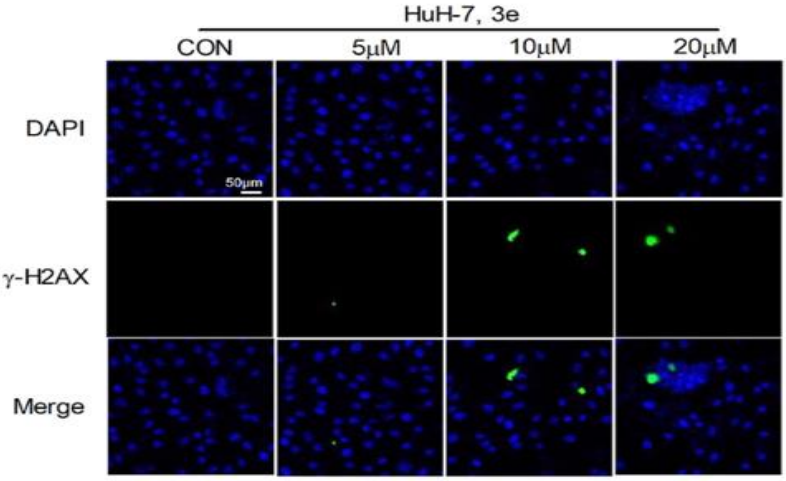


b)

**Figure 7.** (a) Cells treated with 5 μM, 10 μM, or 20 μM of 3c for 24 h; damaged DNA appears green, nuclei blue.
(b) Same staining pattern for cells exposed to 5 μM, 10 μM, or 20 μM of 3e for 24 h.
n = 5–6.

*Effects of compounds 3c and 3e on autophagy*

To examine autophagy involvement, Huh-7 cells were treated with 5, 10, or 20 μM of either compound for 24 h. Autophagosome formation was then monitored using MDC, a fluorescent probe that selectively labels autophagic vesicles. A marked increase in MDC-positive puncta was evident with both molecules **(Figure 8)**, implying that 3c and 3e actively promote autophagic processes that may contribute to loss of tumor-cell viability.

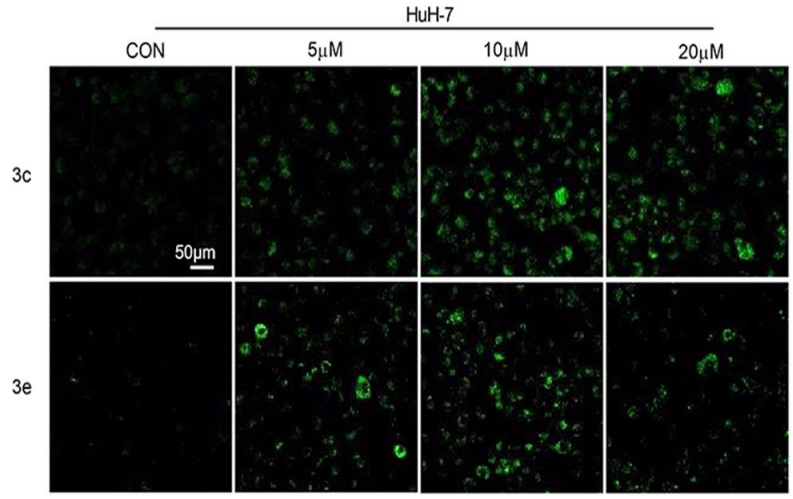


**Figure 8** Autophagy visualization in Huh-7 cells after 24 h exposure to 5 μM, 10 μM, or 20 μM of compounds 3c or 3e.
n = 5–6.

*Acute oral toxicity assessment*

Safety evaluation was performed in mice receiving compound 3c under acute-toxicity testing conditions. Throughout the 14-day monitoring interval, no deaths or notable pathological symptoms were detected. Body-weight records showed no meaningful deviation from vehicle-treated controls at any measured point. Post-study examinations—including organ-weight ratios and histological inspection of the heart, liver, spleen, lungs, and kidneys—revealed no abnormal findings attributable to 3c. Collectively, these observations indicate a favorable short-term safety profile, as summarized in **Figure 9**.

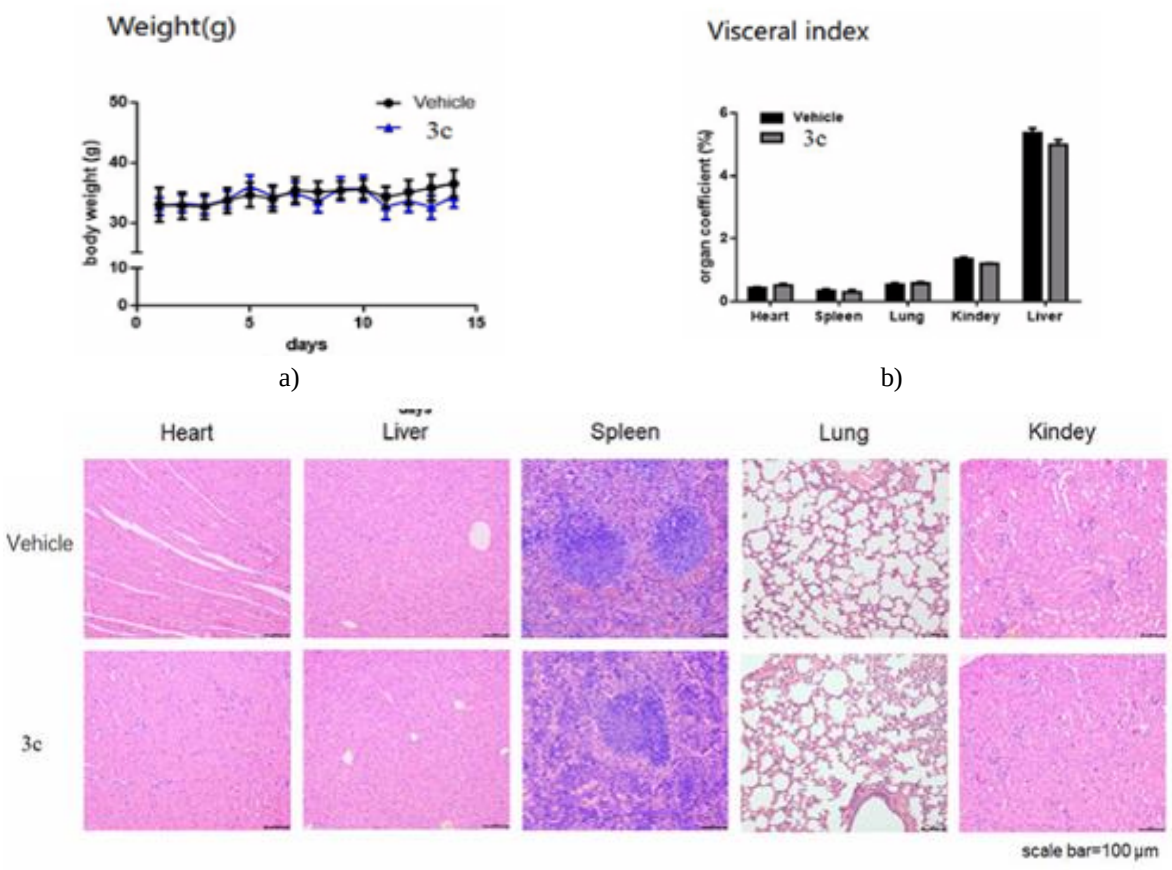


**Figure 9.** (a) Changes in mouse body weight.
(b) Organ assessments following acute-toxicity exposure.
(c) H&E staining of major organs from mice treated with compound 3c.
Data represent Mean ± SEM, statistical comparisons via two-tailed Student's t-test, $P < 0.05$, $n = 5–6$.

In this work, we generated a new panel of diarylurea/1,2,3-triazole hybrids using nucleophilic addition followed by 1,3-dipolar cycloaddition. These molecules displayed selective anticancer behavior in vitro across several malignant cell models, with the strongest growth-suppressive responses appearing in Huh-7 hepatocellular carcinoma cells. Within the library, 3c and 3e stood out due to their enhanced inhibition of Huh-7 proliferation, favorable selectivity ratios, and suitable physicochemical properties for drug development. Mechanistic exploration indicated that these triazole–urea scaffolds operate through multiple pathways, including induction of genomic injury, suppression of cell-cycle progression, and stimulation of apoptotic and autophagy-related death mechanisms. Additionally, in vivo acute-toxicity evaluation confirmed that the compounds were well tolerated. Overall, this study highlights the therapeutic potential of diarylurea–1,2,3-triazole hybrids for treating hepatocellular carcinoma and provides useful guidance for further anticancer drug discovery.

## Conclusion

In this work, we generated a new panel of diarylurea/1,2,3-triazole hybrids using nucleophilic addition followed by 1,3-dipolar cycloaddition. These molecules displayed selective anticancer behavior in vitro across several malignant cell models, with the strongest growth-suppressive responses appearing in Huh-7 hepatocellular carcinoma cells. Within the library, 3c and 3e stood out due to their enhanced inhibition of Huh-7 proliferation, favorable selectivity ratios, and suitable physicochemical properties for drug development. Mechanistic exploration indicated that these triazole–urea scaffolds operate through multiple pathways, including induction of genomic injury, suppression of cell-cycle progression, and stimulation of apoptotic and autophagy-related death mechanisms. Additionally, in vivo acute-toxicity evaluation confirmed that the compounds were well tolerated.

Overall, this study highlights the therapeutic potential of diarylurea–1,2,3-triazole hybrids for treating hepatocellular carcinoma and provides useful guidance for further anticancer drug discovery.

*Experimental work*

*Materials and chemistry*

The 1,2,3-triazole intermediate was prepared by our laboratory. All reagents came from commercial sources, and solvents were freshly distilled before reaction. Reaction progress was monitored using TLC on 0.25 mm silica gel plates (60GF-254) detected under UV or with ferric chloride. Products were isolated through column chromatography on 200–300 mesh silica. NMR spectra were recorded on a Bruker Avance 400 MHz instrument; chemical shifts (δ) are reported in ppm and coupling constants (J) in Hz, using TMS as the reference. High-resolution ESI-MS data were collected using an API 4000 mass spectrometer. All DMSO-d6 solutions were used for NMR analyses. Melting points were determined on an electrothermal instrument without correction. FTIR spectra were acquired using a Brukar FTIR device.

*General preparation of compound 2a*

*(Applicable to 2b–2c, 4a–4b, and 6a–6c)*

A solution of 4-chlorophenyl isocyanate (200 mg, 1.3 mmol) in $CH_2Cl_2$ (10 mL) was treated with 3-aminophenylacetylene (152 mg, 1.3 mmol) in a single addition. The reaction mixture was stirred for 2.5 h at room temperature, concentrated, and purified using silica-gel column chromatography (PE/EA = 3:1) to yield 2a (316 mg, 90%).

Mp: 212.0–212.4°C.

$^1$H NMR (400 MHz, DMSO-$d_6$) δ: 8.87 (s, 1H), 8.82 (s, 1H), 7.66 (s, 1H), 7.49 (d, J = 8.9 Hz, 2H), 7.40 (d, J = 1.2 Hz, 1H), 7.36–7.27 (m, 3H), 7.09 (dt, J = 7.6, 1.3 Hz, 1H), 4.16 (s, 1H).

$^{13}$C NMR (100 MHz, DMSO-$d_6$): 152.8, 140.3, 139.0, 129.7, 129.1, 126.0, 125.7, 122.5, 121.5, 120.3, 119.5, 84.0, 80.9.

IR (KBr): ν 3350, 3180 (s, N–H), 2900 (w, C–H), 1680 (vs, C=O, amide I), 1600 (s, amide II), 1280 (m, C–N, amide III) $cm^{-1}$.

HRMS (ESI) m/z: calcd for $C_{15}H_{12}ClN_2O$ $[M+H]^+$ 271.0613, found 271.0627.

*1-(2-Bromophenyl)-3-(3-Ethynylphenyl)urea (2b)*

White solid, yield 85%, Mp 170.0–172.0°C.

$^1$H NMR (400 MHz, DMSO-$d_6$) δ: 9.57 (s, 1H), 8.17 (s, 1H), 8.05 (dd, J = 8.3, 1.6 Hz, 1H), 7.70 (d, J = 1.9 Hz, 1H), 7.62 (dd, J = 8.0, 1.5 Hz, 1H), 7.46–7.26 (m, 3H), 7.14–7.08 (m, 1H), 6.99 (ddd, J = 8.1, 7.3, 1.6 Hz, 1H), 4.17 (s, 1H).

$^{13}$C NMR (100 MHz, DMSO-$d_6$): 159.1, 153.0, 140.4, 136.3, 129.7, 125.6, 122.5, 121.5, 120.7, 120.6, 119.4, 115.9, 115.7, 84.1, 80.8.

IR: ν 3280 (s, N–H), 3080 (w), 1650 (vs, C=O), 1550 (s), 1250 (m), 650 (m, C–Br) $cm^{-1}$.

HRMS (ESI) m/z: calcd for $C_{15}H_{12}BrN_2O$ $[M+H]^+$ 315.0128, found 315.0129.

*1-(4-Chlorophenyl)-3-(4-Ethynylphenyl)urea (4a)*

White solid, yield 86%, Mp 265.5–266.5°C.

$^1$H NMR (400 MHz, DMSO-$d_6$) δ: 8.90 (d, J = 17.5 Hz, 2H), 7.51–7.45 (m, 4H), 7.41 (d, 2H), 7.34 (d, J = 8.9 Hz, 2H), 4.05 (s, 1H).

$^{13}$C NMR: 152.7, 140.7, 138.9, 132.9, 129.1, 126.0, 120.3, 118.5, 115.2, 84.2, 79.9.

IR: ν 3250 (s), 2905 (w), 1690 (vs), 1660 (s), 1260 (m) $cm^{-1}$.

HRMS: calculated 271.0613, found 271.0640.

*1-(2-Bromophenyl)-3-(4-Ethynylphenyl)urea (4b)*

White solid, yield 88%, Mp 217.0–218.0°C.

$^1$H NMR δ: 9.65 (s, 1H), 8.20 (s, 1H), 8.05 (dd, J = 8.3, 1.6 Hz, 1H), 7.63 (dd, J = 8.0, 1.5 Hz, 1H), 7.54–7.46 (m, 2H), 7.43–7.40 (m, 2H), 7.35 (ddd, J = 8.5, 7.3, 1.5 Hz, 1H), 7.00 (td, J = 7.7, 1.6 Hz, 1H), 4.06 (s, 1H).

$^{13}$C NMR: 152.4, 140.6, 137.3, 133.0, 132.9, 128.6, 124.8, 122.9, 118.4, 115.4, 113.8, 84.2, 80.0.

IR: ν 3260, 3160, 1600, 1560, 1270, 655 $cm^{-1}$.

HRMS: calcd 315.0128, found 315.0124.

*1-(4-Chlorophenyl)-3-(Prop-2-yn-1-yl)urea (6a)*
White solid, yield 89%, Mp 195.0–196.5°C.
$^{1}$H NMR δ: 8.73 (s, 1H), 7.43 (d, J = 8.9 Hz, 2H), 7.27 (d, J = 8.9 Hz, 2H), 6.51 (t, J = 5.7 Hz, 1H), 3.88 (dd, J = 5.7, 2.5 Hz, 2H), 3.11 (s, 1H).
$^{13}$C NMR: 155.1, 139.7, 129.0, 125.3, 119.8, 82.5, 73.3, 29.2.
IR: 3300, 3190, 3050, 1680, 1590, 1490, 1450, 1300, 750 cm$^{-1}$.
HRMS: calcd 209.0476, found 209.0476.

*1-(2-Bromophenyl)-3-(Prop-2-yn-1-yl)urea (6b)*
White solid, yield 86%, Mp 178.4–179.5°C.
$^{1}$H NMR δ: 8.03 (dd, J = 8.3, 1.6 Hz, 1H), 7.93 (s, 1H), 7.57 (dd, J = 8.0, 1.5 Hz, 1H), 7.41 (t, J = 5.5 Hz, 1H), 7.29 (ddd, J = 8.5, 7.4, 1.5 Hz, 1H), 6.92 (td, J = 7.6, 1.6 Hz, 1H), 3.92 (dd, J = 5.5, 2.5 Hz, 2H), 3.16 (t, J = 2.5 Hz, 1H).
$^{13}$C NMR: 154.9, 138.0, 132.9, 128.5, 124.0, 122.3, 113.0, 82.1, 73.7, 29.2.
IR: 3350, 3250, 3050, 1690, 1690, 760 cm$^{-1}$.
HRMS: calcd 252.9971, found 252.9972.

*General method for obtaining compound 3a*
Compound 2a (100 mg, 0.37 mmol) was combined with 1-(azidomethyl)-4-chlorobenzene (70 mg, 0.42 mmol) in a 10 mL ternary solvent mixture consisting of water, tert-butanol, and THF (1:1:1). Copper sulfate pentahydrate (10 mg, 0.04 mmol) and sodium ascorbate (14 mg, 0.07 mmol) were introduced as catalytic additives. The suspension was kept at 85 °C, and its progress was assessed via TLC. Once the reaction reached completion, extraction was performed with dichloromethane (3 × 15 mL). The organic phase was rinsed sequentially with water and brine, dried with anhydrous sodium sulfate, and evaporated under reduced pressure. The crude material was purified through silica gel chromatography (DCM/MeOH, 30:1), giving compound 3a.

*1-(3-(1-(4-Chlorobenzyl)-1H-1,2,3-Triazol-4-yl)phenyl)-3-(4-Chlorophenyl)urea (3a)*
White crystalline product, 83% yield, mp 227.5–230.5 °C.
1H NMR (400 MHz, DMSO-d6) δ 8.86 (s, 2H), 8.62 (s, 1H), 8.04 (s, 1H), 7.53–7.22 (m, 11H), 5.66 (s, 2H).
13C NMR (100 MHz, DMSO-d6) δ 152.9, 147.9, 147.8, 140.6, 139.1, 135.5, 133.4, 131.6, 130.4, 129.9, 129.1, 125.9, 122.1, 120.3, 119.5, 118.4, 115.4, 52.7.
IR (KBr): 3435, 3320, 3215 (br, NH/OH), 1705 (vs, C=O), 1605 (m, C=N), 1490 (m, C=C), 1250 (s, C-N), 830 (s, C-Cl) cm$^{-1}$.
HRMS (ESI) m/z: calcd for C22H17Cl2N5NaO [M+Na]+ 460.0702; found 460.0763.

*1-(3-(1-(3-Chlorobenzyl)-1H-1,2,3-Triazol-4-yl)phenyl)-3-(4-Chlorophenyl)urea (3b)*
White solid, 78% yield, mp 217.0–220.0 °C.
1H NMR (400 MHz, DMSO-d6) δ 8.84 (s, 2H), 8.66 (s, 1H), 8.05 (s, 1H), 7.52–7.51 (m, 1H), 7.50–7.49 (m, 1H), 7.48–7.46 (m, 1H), 7.46–7.40 (m, 3H), 7.38–7.30 (m, 5H), 5.67 (s, 2H).
13C NMR (100 MHz, DMSO-d6) δ 152.9, 147.2, 140.6, 139.1, 138.9, 133.8, 131.6, 131.2, 129.9, 129.1, 128.7, 128.4, 127.2, 125.9, 122.2, 120.3, 119.5, 118.4, 115.4, 52.7.
IR (KBr): 3120 (br, NH/OH), 1710 (vs, C=O), 1665 (m, C=N), 1480 (m, C=C), 1350 (s, C-N), 800 (s, C-Cl) cm$^{-1}$.
HRMS (ESI) m/z: calcd 460.0702; found 460.0763.

*1-(3-(1-(4-Bromobenzyl)-1H-1,2,3-Triazol-4-yl)phenyl)-3-(4-Chlorophenyl)urea (3c)*
White solid, 79% yield, mp 233.0–236.5 °C.
1H NMR (400 MHz, DMSO-d6) δ 8.84 (s, 2H), 8.61 (s, 1H), 8.04 (d, J = 1.9 Hz, 1H), 7.60 (d, J = 8.4 Hz, 2H), 7.51 (d, J = 8.9 Hz, 2H), 7.47–7.27 (m, 7H), 5.64 (s, 2H).
13C NMR δ 152.9, 147.2, 140.6, 139.2, 135.9, 133.5, 132.2, 131.6, 130.7, 129.9, 129.19, 125.9, 122.1, 121.9, 120.3, 118.4, 115.4, 52.7.
IR: 3455, 3265 (br, NH/OH), 1710 (vs), 1665 (m), 1590 (m), 1250 (s), 750 (m, C-Br) cm$^{-1}$.

HRMS m/z: calcd 482.0378; found 482.0389.

*1-(2-Bromophenyl)-3-(3-(1-(4-Chlorobenzyl)-1H-1,2,3-Triazol-4-yl)phenyl)urea (3d)*
White material, 88% yield, mp 206.0–208.0 °C.
1H NMR δ 9.60 (s, 1H), 8.62 (s, 1H), 8.18–7.99 (m, 3H), 7.61 (d, J = 1.5 Hz, 1H), 7.50–7.26 (m, 8H), 6.99 (td, J = 7.6, 1.6 Hz, 1H), 5.66 (s, 2H).
13C NMR δ 152.6, 147.1, 140.5, 137.5, 135.5, 133.4, 133.0, 131.7, 130.4, 130.0, 129.3, 128.6, 124.6, 122.7, 122.1, 119.6, 118.2, 115.2, 113.5, 52.7.
IR: 3545, 3250, 1715, 1675, 1570, 820, 750 $cm^{-1}$.
HRMS: calcd 482.0378; found 482.0387.

*1-(3-(1-(4-Bromobenzyl)-1H-1,2,3-Triazol-4-yl)phenyl)-3-(2-Bromophenyl)urea (3e)*
White solid, 85% yield, mp 211.5–213.5 °C.
1H NMR δ 9.61 (s, 1H), 8.62 (s, 1H), 8.17–8.01 (m, 3H), 7.71–7.57 (m, 3H), 7.47–7.25 (m, 6H), 7.00 (dd, J = 7.7, 1.6 Hz, 1H), 5.64 (s, 2H).
13C NMR δ 152.6, 147.1, 144.7, 135.9, 134.9, 133.0, 132.0, 131.7, 130.7, 130.0, 128.6, 124.6, 122.7, 122.1, 121.9, 119.6, 118.2, 115.2, 113.5, 52.7.
IR: 3340, 3200, 1680, 1675, 1570, 755 $cm^{-1}$.
HRMS: calcd 525.9873; found 525.9868.

*1-(4-(1-(4-Chlorobenzyl)-1H-1,2,3-Triazol-4-yl)phenyl)-3-(4-Chlorophenyl)urea (5a)*
White solid, 90% yield, mp 196.5–197.4 °C.
1H NMR δ 8.83 (d, J = 11.9 Hz, 2H), 8.53 (s, 1H), 7.76 (d, J = 8.5 Hz, 2H), 7.59–7.42 (m, 6H), 7.42–7.27 (m, 4H), 5.65 (s, 2H).
13C NMR δ 152.8, 147.2, 139.8, 139.1, 135.5, 130.3, 129.3, 129.2, 129.1, 126.3, 125.9, 124.9, 121.2, 120.2, 119.0, 52.6.
IR: 3320, 3215, 1705, 1605, 1490, 1250, 790 $cm^{-1}$.
HRMS: calcd 460.0702; found 460.0763.

*1-(4-(1-(3-Chlorobenzyl)-1H-1,2,3-Triazol-4-yl)phenyl)-3-(4-Chlorophenyl)urea (5b)*
White solid, 94% yield, mp 195.5–196.5 °C.
1H NMR δ 8.94 (d, J = 11.5 Hz, 2H), 8.57 (s, 1H), 7.76 (d, J = 8.3 Hz, 2H), 7.52 (dd, J = 13.0, 8.6 Hz, 4H), 7.48–7.41 (m, 3H), 7.35–7.27 (m, 3H), 5.67 (s, 2H).
13C NMR δ 152.9, 147.2, 140.6, 139.2, 138.8, 133.8, 131.2, 129.1, 128.6, 128.3, 127.1, 126.3, 125.8, 124.6, 123.0, 121.5, 120.2, 119.0, 52.7.
IR: 3310, 3217, 1735, 1615, 1590, 1250, 795 $cm^{-1}$.
HRMS: calcd 460.0702; found 460.0763.

*1-(4-(1-(4-Bromobenzyl)-1H-1,2,3-Triazol-4-yl)phenyl)-3-(4-Chlorophenyl)urea (5c)*
White solid, 91% yield, mp 238.5–240.6 °C.
1H NMR δ 8.83 (d, J = 11.9 Hz, 2H), 8.53 (s, 1H), 7.76 (d, J = 8.6 Hz, 2H), 7.60 (d, J = 8.4 Hz, 2H), 7.54–7.46 (m, 4H), 7.36–7.16 (m, 4H), 5.63 (s, 2H).
13C NMR δ 152.8, 147.2, 139.8, 139.1, 135.9, 132.2, 130.6, 129.1, 126.3, 125.9, 124.9, 121.9, 121.3, 120.2, 119.0, 52.7.
IR: 3540, 3251, 1716, 1685, 1575, 790, 750 $cm^{-1}$.
HRMS: calcd 482.0378; found 482.0392.

*1-(2-Bromophenyl)-3-(4-(1-(4-Chlorobenzyl)-1H-1,2,3-triazol-4-yl)phenyl)urea (5d)*
Appears as a white solid with an 85% yield and melts at 213.5–214.4 °C.
$^1$H NMR (400 MHz, DMSO-$d_6$): δ 9.57 (s, 1H), 8.54 (s, 1H), 8.17 (s, 1H), 8.08 (dd, J = 8.3, 1.6 Hz, 1H), 7.81–7.76 (m, 2H), 7.63 (dd, J = 8.0, 1.5 Hz, 1H), 7.55 (d, J = 8.7 Hz, 2H), 7.47 (d, J = 8.5 Hz, 2H), 7.41–7.30 (m, 3H), 7.00 (dd, J = 7.7, 1.6 Hz, 1H), 5.65 (s, 2H).

$^{13}$C NMR (100 MHz, DMSO-$d_6$): δ 152.6, 147.1, 135.5, 133.3, 133.2, 133.0, 130.3, 129.3, 128.6, 126.3, 125.0, 124.6, 122.8, 121.3, 121.2, 118.9, 113.6, 52.7.
IR (KBr): ν = 3340, 3261 (broad, NH/OH), 1700 (strong, C=O), 1685 (medium, C=N), 1575 (medium, C=C), 795 (strong, C–Cl), 755 (medium, C–Br).
HRMS (ESI): m/z calculated 482.0378, observed 482.0386.

*1-(4-(1-(4-Bromobenzyl)-1H-1,2,3-triazol-4-yl)phenyl)-3-(2-bromophenyl)urea (5e)*
Retrieved as a white material in 76% yield, melting 204.5–206.5 °C.
$^{1}$H NMR (400 MHz, DMSO-$d_6$): δ 9.57 (s, 1H), 8.54 (s, 1H), 8.17–8.07 (m, 2H), 7.78 (d, J = 8.2 Hz, 2H), 7.65–7.49 (m, 5H), 7.41–7.21 (m, 3H), 6.99 (t, J = 7.7 Hz, 1H), 5.63 (s, 2H).
$^{13}$C NMR: δ 152.6, 147.1, 139.7, 137.5, 135.9, 133.0, 132.2, 130.6, 128.6, 126.3, 124.9, 124.6, 122.7, 121.9, 121.3, 118.9, 113.7, 52.7.
IR: ν = 3240, 3255 (broad NH/OH), 1680 (very strong C=O), 1685 (C=N), 1575 (C=C), 765 (C–Br).
HRMS: calc. 525.9873, found 525.9864.

*1-((1-(4-Chlorobenzyl)-1H-1,2,3-triazol-4-yl)methyl)-3-(4-chlorophenyl)urea (7a)*
White crystalline compound; 88% yield, Mp 198.2–199.3 °C.
$^{1}$H NMR (400 MHz): δ 8.70 (s, 1H), 8.03 (s, 1H), 7.43 (dd, J = 10.2, 8.1 Hz, 4H), 7.34 (d, J = 8.5 Hz, 2H), 7.26 (d, J = 8.8 Hz, 2H), 6.63 (s, 1H), 5.58 (s, 2H), 4.32 (d, J = 5.3 Hz, 2H).
$^{13}$C NMR: δ 157.2, 155.4, 139.8, 135.6, 132.4, 133.3, 130.4, 129.2, 128.9, 125.1, 119.6, 52.4, 35.3.
IR: ν = 3180 (N–H), 1680 (C=O), 1600 (aromatic C=C), 1300 (C–N), 1050 (N–N), 750 (C–Cl).
HRMS: calc. 376.0726, found 376.0724.

*1-((1-(3-Chlorobenzyl)-1H-1,2,3-triazol-4-yl)methyl)-3-(4-chlorophenyl)urea (7b)*
White solid; 87% yield; melting 191.5–192.5 °C.
$^{1}$H NMR: δ 8.71 (s, 1H), 8.06 (s, 1H), 7.56–7.36 (m, 5H), 7.30–7.21 (m, 3H), 6.64 (t, J = 5.8 Hz, 1H), 5.60 (s, 2H), 4.33 (d, J = 5.5 Hz, 2H).
$^{13}$C NMR: δ 155.4, 139.8, 139.0, 133.8, 133.7, 131.2, 128.9, 128.6, 128.3, 127.2, 125.1, 124.5, 119.7, 52.4, 35.3.
IR: ν = 3170 (N–H), 1580 (C=O), 1605 (aromatic C=C), 1300 (C–N), 1050 (N–N), 780 (C–Cl).
HRMS: calc. 376.0726, found 376.0725.

*1-((1-(4-Bromobenzyl)-1H-1,2,3-triazol-4-yl)methyl)-3-(4-chlorophenyl)urea (7c)*
White material; 79% yield; Mp 197.5–198.6 °C.
$^{1}$H NMR: δ 8.70 (s, 1H), 8.02 (s, 1H), 7.58 (d, J = 8.4 Hz, 2H), 7.42 (d, J = 8.9 Hz, 2H), 7.30–7.20 (m, 4H), 6.63 (t, J = 5.6 Hz, 1H), 5.56 (s, 2H), 4.32 (d, J = 5.6 Hz, 2H).
$^{13}$C NMR: δ 164.0, 155.4, 139.8, 136.0, 132.1, 130.7, 128.9, 125.1, 123.3, 121.9, 119.6, 52.4, 35.3.
IR: ν = 3165 (N–H), 1680 (C=O), 1605 (C=C), 1310 (C–N), 1050 (N–N), 760 (C–Cl).
HRMS: calc. 420.0221, found 420.0221.

*1-(2-Bromophenyl)-3-((1-(4-chlorobenzyl)-1H-1,2,3-triazol-4-yl)methyl)urea (7d)*
White crystalline species; 87% yield, Mp 205.5–206.5 °C.
$^{1}$H NMR: δ 8.13–8.01 (m, 2H), 7.92 (s, 1H), 7.59–7.49 (m, 2H), 7.49–7.41 (m, 2H), 7.35 (d, J = 8.4 Hz, 2H), 7.28 (t, J = 7.9 Hz, 1H), 6.90 (td, J = 7.6, 1.6 Hz, 1H), 5.60 (s, 2H), 4.34 (d, J = 5.5 Hz, 2H).
$^{13}$C NMR: δ 172.9, 155.1, 138.2, 135.6, 133.3, 132.8, 130.4, 129.2, 128.4, 123.8, 123.5, 122.1, 112.7, 52.4, 35.3.
IR: ν = 3180 (N–H), 1675 (C=O), 1580 (C=C), 1310 (C–N), 1050 (N–N).
HRMS: calc. 420.0221, found 420.0227.

*1-((1-(4-Bromobenzyl)-1H-1,2,3-triazol-4-yl)methyl)-3-(2-bromophenyl)urea (7e)*
Recovered as a white solid, 85% yield, melting 188.6–188.7 °C.
$^{1}$H NMR: δ 8.08–8.00 (m, 2H), 7.92 (s, 1H), 7.61–7.47 (m, 4H), 7.32–7.25 (m, 3H), 6.90 (t, J = 7.2 Hz, 1H), 5.57 (s, 2H), 4.34 (d, J = 5.6 Hz, 2H).
$^{13}$C NMR: δ 155.2, 138.7, 138.1, 136.0, 132.8, 132.1, 130.7, 128.4, 123.9, 122.1, 121.9, 118.2, 112.8, 52.5, 35.3.
IR: ν = 3170 (N–H), 1680 (C=O), 1620 (C=C), 1305 (C–N), 1150 (N–N), 760 (C–Br).

HRMS: calc. 463.9716, found 463.9715.

*Biological materials*

DMSO was sourced from Sigma-Aldrich (St. Louis, Missouri, USA).
DMEM, RPMI-1640, FBS, and penicillin–streptomycin were acquired from Gibco (Grand Island, NY, USA).
Cell Counting Kit-8, the Calcein/PI live–dead staining set, kits for DNA damage analysis, and autophagy markers originated from Beyotime Biotechnology (Shanghai, China).
The Annexin V-FITC/PI apoptosis kit came from BD Biosciences (Franklin Lake, New Jersey, USA).

*Cell culture*

Human lung cancer lines (H460, H1299, A549, PC-9), the hepatocellular carcinoma line Huh-7, breast cancer cells MCF-7, and L02 cells were sourced from ATCC. Cells were maintained in DMEM or RPMI-1640 supplemented with 10% FBS plus 1% penicillin/streptomycin. Cultures were kept at 37 °C in a humidified 5% $CO_2$ environment.

*Cell viability and $IC_{50}$ evaluation*

Cell survival was assessed using a CCK-8 kit. A total of $3 \times 10^3$ cells were plated per well in 96-well plates. Once attached (overnight), cells received either 20 μM or 50 μM of the test compounds, or DMSO vehicle, for 48 h or 72 h. Afterward, CCK-8 reagent was added, and plates were incubated for 1 h at 37 °C/5% $CO_2$. Absorbance at 450 nm was read on a Thermo microplate reader, and viability was expressed relative to the untreated group.
For $IC_{50}$ calculations, cells were exposed for 72 h to a range of concentrations (0, 10 μM, 20 μM, 40 μM, 80 μM). Inhibition was derived from viability percentages, and $IC_{50}$ values were generated using GraphPad Prism. Each CCK-8 condition included >5 replicates. Mean ± SE was reported, and group differences were examined with one-way ANOVA followed by Dunnett's post-hoc test (significance threshold $P < 0.05$).

*Live/dead staining*

Huh-7 cells ($3 \times 10^3$/well) were seeded in 96-well plates. After overnight adherence, cultures were exposed to 0, 5 μM, 10 μM, or 20 μM compound for 24 h. A LIVE/DEAD kit was then used to label viable and non-viable cells, which were visualized by fluorescence microscopy. Replicates numbered 5–6 per group.

*Apoptosis assay*

Huh-7 cells were plated in 6-well dishes at $3 \times 10^5$ cells/well. Following overnight attachment, cells were treated for 72 h with 0, 5 μM, 10 μM, or 20 μM of the compounds. Cells were harvested and stained with Annexin V-FITC and PI. Apoptosis rates were quantified using a BD flow cytometer and analyzed in FlowJo v10. Data were presented as Mean ± SE. One-way ANOVA with Dunnett's comparison was used ($P < 0.05$ significant). Experiments involved 5–6 replicates per condition.

*RT-PCR analysis*

Huh-7 cells grown in 12-well plates were treated with 10 μM compound for 72 h. RNA was isolated via TRIzol (Ambion), and RT-PCR was conducted using PowerUp SYBR Green Master Mix (ABI). GAPDH served as the reference gene. Primers (Sangon Biotech, Shanghai) are shown in **Table 5**. Data (Mean ± SEM) were evaluated with a two-tailed Student's t-test, with $P < 0.05$ considered significant. Six replicates were performed per group.

**Table 5.** Oligonucleotide Primer Pairs Used for RT-PCR

| Gene | Forward Primer (5′→3′) | Reverse Primer (5′→3′) |
|---|---|---|
| P53 | CCTCAGCATCTTATCCGAGTGG | TGGATGGTGGTACAGTCAGAGC |
| P21 | AGGTGGACCTGGAGACTCTCAG | TCCTCTTGGAGAAGATCAGCCG |
| H2AX | CGGCAGTGCTGGAGTACCTCA | AGCTCCTCGTCGTTGCGGATG |
| Bax | TCAGGATGCGTCCACCAAGAAG | TGTGTCCACGGCGGCAATCATC |
| Bcl2 | ATCGCCCTGTGGATGACTGAGT | GCCAGGAGAAATCAAACAGAGGC |
| Caspase3 | GGAAGCGAATCAATGGACTCTGG | GCATCGACATCTGTACCAGACC |

| | | |
|---|---|---|
| Caspase6 | AGGTGGATGCAGCCTCCGTTTA | ATGAGCCGTTCACAGTTTCCCG |
| Caspase7 | CGGAACAGACAAAGATGCCGAG | AGGCGGCATTTGTATGGTCCTC |
| Keap1 | CAACTTCGCTGAGCAGATTGGC | TGATGAGGGTCACCAGTTGGCA |
| Nrf2 | AGGTTGCCCACATTCCCAAA | ACGTAGCCGAAGAAACCTCA |
| Gpx4 | TTGGTCGGCTGGACGAGG | GGGACGCGCACATGGT |
| Tnfa | ACTGAAAGCATGATCCGGGACG | AGCAGGCAGAAGAGCGTGGTGG |
| ATG5 | GGATGGGATTGCAAAATGACAGA | TCCTAGTGTGTGCAACTGTCC |
| ATG7 | GGCCAATAAGATGGGTCTGA | GCTTTTGTCCACTGCTCCTC |

*Western blotting*

Protein profiling was performed by Western blot. Huh-7 cells in 12-well plates received 10 μM compound for 72 h. Total protein was extracted using RIPA buffer containing protease/phosphatase inhibitors (CST). Antibodies included caspase-3, caspase-9, γH2AX, PARP, cyclin D, cyclin E, LC3, and β-actin (all CST). Values were shown as Mean ± SEM. A Student's t-test was applied ($P < 0.05$). Each condition had 6 replicates.

*DNA damage staining*

Huh-7 cells ($3 \times 10^3$/well) were plated in 96-well dishes. After treatment with 0, 5 μM, 10 μM, or 20 μM for 24 h, the DNA damage reagent was applied. Nuclei were counterstained in blue, while damaged DNA appeared green. Imaging was done by fluorescence microscopy. Each condition included 5–6 replicates.

*Autophagy assay*

Huh-7 cells ($3 \times 10^3$/well) were cultured in 96-well plates and exposed to 0, 5 μM, 10 μM, or 20 μM for 24 h. After removing the medium, monodansylcadaverine staining was conducted for 1 h at 37 °C in the dark. Confocal microscopy was used for visualization. Replicates numbered 5–6 per group.

*In vivo experiments*

*Animals*

Eight-week-old SPF Kunming mice were obtained from Henan Skbex Biotechnology Co., Ltd. (SCXK (Yu) 2020-0005). Husbandry was under a 12-h light/dark cycle with unrestricted water access and a 7-day acclimation period. After toxicity studies, euthanasia was carried out by intraperitoneal pentobarbital (150 mg/kg). Ethical approval was granted by the Animal Ethics Committee of Henan University of Science and Technology (HAUST-024-M081001, October 17, 2024).

*Acute toxicity assessment*

Female KM mice (8 weeks old; n=6/group) were randomized into a vehicle control and a 3c-treated group. Controls received the vehicle mixture (5% DMSO + 40% PEG300 + 1% Tween-80 + 54% saline) by gavage, while the treated group received 3c at 500 mg/kg. Body mass and overall appearance were monitored over 14 days. Major organs (heart, liver, spleen, lungs, kidneys) were weighed to compute organ coefficients (organ weight/body weight × 100%). Organs were preserved in 10% formaldehyde, paraffin embedded, sectioned, and stained with H&E. Comparisons used Student's t-tests, with significance at $P < 0.05$.

*Statistical analyses*

GraphPad Prism 9.5 was used for all analyses. One-way ANOVA with Dunnett's post-test was applied for comparisons across multiple groups, while two-group analyses used Student's t-tests. All datasets were generated from at least three independent experiments. Statistical significance was defined as $P < 0.05$.

**Acknowledgments:** None

**Conflict of Interest:** None

**Financial Support:** None

**Ethics Statement:** None

## References


1. Siegel RL, Miller KD, Jemal A. Cancer Statistics, 2017. CA-A Cancer J Clin. 2017;67(1):7–30. doi:10.3322/caac.21387
2. Sung H, Ferlay J, Siegel RL, Laversanne M, Soerjomataram I, Jemal A, et al. Global cancer statistics 2020: GLOBOCAN estimates of incidence and mortality worldwide for 36 cancers in 185 countries. CA-A Cancer J Clin. 2021;71(3):209–49. doi:10.3322/caac.21660
3. Chen S, Cao Z, Prettner K, Kuhn M, Yang J, Jiao L, et al. Estimates and projections of the global economic cost of 29 cancers in 204 countries and territories from 2020 to 2050. JAMA Oncol. 2023;9(Bray4):465–72. doi:10.1001/jamaoncol.2022.7826
4. Shabbits JA, Krishna R, Mayer LD. Molecular and pharmacological strategies to overcome multidrug resistance. Expert Rev Anticancer Therapy. 2001;1(4):585–94. doi:10.1586/14737140.1.4.585
5. Kurt Yilmaz N, Schiffer CA. Introduction: drug resistance. Chem Rev. 2021;121(6):3235–7. doi:10.1021/acs.chemrev.1c00118
6. Wu J, Lin Z. Non-small cell lung cancer targeted therapy: drugs and mechanisms of drug resistance. Int J Mol Sci. 2022;23(23):15056. doi:10.3390/ijms232315056
7. Zhao S, Liu J, Lv Z, Zhang G, Xu Z. Recent updates on 1,2,3-triazole-containing hybrids with in vivo therapeutic potential against cancers: a mini-review. Eur J Med Chem. 2023;251:115254. doi:10.1016/j.ejmech.2023.115254
8. Bozorov K, Zhao J, Aisa HA. 1,2,3-Triazole-containing hybrids as leads in medicinal chemistry: a recent overview. CA-A Cancer J Clin. 2019;27(16):3511–31. doi:10.1016/j.bmc.2019.07.005
9. Guan Q, Xing S, Wang L, Zhu J, Guo C, Xu C, et al. Triazoles in medicinal chemistry: physicochemical properties, bioisosterism, and application. J Med Chem. 2024;67(10):7788–824. doi:10.1021/acs.jmedchem.4c00652
10. Bonandi E, Christodoulou MS, Fumagalli G, Perdicchia D, Rastelli G, Passarella D. The 1,2,3-triazole ring as a bioisostere in medicinal chemistry. Drug Discov Today. 2017;22(10):1572–81. doi:10.1016/j.drudis.2017.05.014
11. Ronchetti R, Moroni G, Carotti A, Gioiello A, Camaioni E. Recent advances in urea- and thiourea-containing compounds: focus on innovative approaches in medicinal chemistry and organic synthesis. Rsc Med Chem. 2021;12(7):1046–64. doi:10.1039/d1md00058f
12. Li H-Q, Lv P-C, Yan T, Zhu H-L. Urea derivatives as anticancer agents. Anti-Cancer Agents Med Chem. 2009;9(4):471–80. doi:10.2174/1871520610909040471
13. Pinheiro Pd SM, Franco LS, Montagnoli TL, Fraga CAM. Molecular hybridization: a powerful tool for multitarget drug discovery. Expert Opin Drug Discov. 2024;19(4):451–70. doi:10.1080/17460441.2024.2322990
14. Gontijo VS, Viegas FP, Ortiz CJ, de Freitas Silva M, Damasio CM, Rosa MC, et al. Molecular hybridization as a tool in the design of multi-target directed drug candidates for neurodegenerative diseases. Curr Neuropharmacol. 2020;18(5):348–407. doi:10.2174/1385272823666191021124443
15. Alkhzem AH, Woodman TJ, Blagbrough IS. Design and synthesis of hybrid compounds as novel drugs and medicines. RSC Adv. 2022;12(30):19470–84. doi:10.1039/D2RA03281C
16. Ivasiv V, Albertini C, Goncalves AE, Rossi M, Bolognesi ML. Molecular hybridization as a tool for designing multitarget drug candidates for complex diseases. Curr Top Med Chem. 2019;19(19):1694–711. doi:10.2174/1568026619666190619115735
17. Bakale RD, Bhagat AN, Mhetre UV, Londhe SV, Rathod SS, Choudhari PB. Design, synthesis and molecular docking study of novel quinoline–triazole molecular hybrids as anticancer agents. J Mole Struct. 2025;1321:140072. doi:10.1016/j.molstruc.2024.140072
18. Mhetre UV, Bhagat AN, Londhe SV, Salunke SS, More RA, Rathod SS, et al. Quinazolinone-linked triazole conjugates: synthesis, biological evaluation, and in silico studies. J Mole Struct. 2025;1331:141594. doi:10.1016/j.molstruc.2025.141594

19. Ma LY, Wang B, Pang LP, Zhang M, Wang SQ, Zheng YC, et al. Design and synthesis of novel 1,2,3-triazole-pyrimidine-urea hybrids as potential anticancer agents. Bioorg Med Chem Lett. 2015;25(5):1124–8. doi:10.1016/j.bmcl.2014.12.087
20. Egile C, Kenigsberg M, Delaisi C, Bégassat F, Do-Vale V, Mestadier J, et al. the selective intravenous inhibitor of the MET tyrosine kinase SAR125844 inhibits tumor growth in MET-amplified cancer. Mol Cancer Ther. 2015;14(2):384–94. doi:10.1158/1535-7163.mct-14-0428
21. Hsu KL, Tsuboi K, Chang JW, Whitby LR, Speers AE, Pugh H, et al. Discovery and optimization of piperidyl-1,2,3-triazole ureas as potent, selective, and in vivo-active inhibitors of α/β-hydrolase domain containing 6 (ABHD6). J Med Chem. 2013;56(21):8270–9. doi:10.1021/jm400899c
22. Duan YC, Zheng YC, Li XC, Wang MM, Ye XW, Guan YY, et al. Design, synthesis and antiproliferative activity studies of novel 1,2,3-triazole-dithiocarbamate-urea hybrids. Eur J Med Chem. 2013;64:99–110. doi:10.1016/j.ejmech.2013.03.058
23. Hou X, Gong X, Mao L, Zhao J, Yang J. Discovery of Novel 1,2,3-triazole Derivatives as IDO1 Inhibitors. Pharmaceuticals. 2022;15(11):1316. doi:10.3390/ph15111316
24. Gao E, Wang Y, Fan GL, Xu G, Wu ZY, Liu ZJ, et al. Discovery of gefitinib-1,2,3-triazole derivatives against lung cancer via inducing apoptosis and inhibiting the colony formation. Sci Rep. 2024;14(1):9223. doi:10.1038/s41598-024-60000-1
25. Liu ZJ, Liu JC, Gao E, Mao LF, Hu S, Li SQ. Synthesis and in vitro antitumor activity evaluation of gefitinib-1,2,3-triazole derivatives. Molecules. 2024;29(4):837. doi:10.3390/molecules29040837